Pramana – J. Phys. (2018) 91:13
https://doi.org/10.1007/s12043-018-1585-2

Numerical simulation of unsteady 3D magneto-Sisko fluid flow with nonlinear thermal radiation and homogeneous–heterogeneous chemical reactions

MASOOD KHAN[1], LATIF AHMAD[1,2,*] and MUHAMMAD AYAZ[3]

[1]Department of Mathematics, Quaid-i-Azam University, Islamabad 44000, Pakistan
[2]Department of Mathematics, Shaheed Benazir Bhutto University, Sheringal, Upper Dir 18000, Pakistan
[3]Department of Mathematics, Abdul Wali Khan University, Mardan, Mardan 23200, Pakistan
*Corresponding author. E-mail: latifahmad@math.qau.edu.pk

MS received 25 October 2017; revised 20 December 2017; accepted 8 January 2018; published online 18 June 2018

Abstract. The chemically reactive unsteady 3D Sisko fluid flow over a bidirectional stretched surface in the presence of nonlinear thermal radiation and magnetic field is considered. The numerical scrutiny of the transformed nonlinear ODEs is performed with the help of a numerical technique known as bvp4c. The mechanism of heat and mass transfer by the applications of chemical reaction and radiation is presented using temperature and concentration graphs. A remarkable enhancing results are estimated in the presence of nonlinear thermal radiation parameter R_d and temperature ratio parameter θ_w for the temperature field. Another significant decreasing outcomes are found while plotting the concentration profile with variation of homogeneous and heterogeneous parameters (k_1, k_2). Computational results of the local skin friction and local Nusselt number are tabulated under the influence of physical parameters which governs the flow. Decrease in skin friction with varying values of λ is observed. On the other hand, the impact of R_d and θ_w on the tabular values of local Nusselt number is found in increasing order. All the graphical results and tabular values are illustrated while testing both cases of power-law fluids including pseudoplastic $(0 < n < 1)$ and dilatant $(n > 1)$ behaviours. A comparison of the bvp4c and shooting technique with RK-45 Fehlberg is presented which shows excellent agreement. Additionally, the present results are compared with the results in the existing literature and both are found to be in very good correlation.

Keywords. Unsteady flow; 3D Sisko fluid; nonlinear thermal radiation; numerical computations.

PACS Nos 44; 44.20.+b; 44.40.+a

Nomenclature

x, y, z	Cartesian coordinates
u, v, w	Velocity components
c_1, d_1, d, β	Constants
t	Time
A, B	Chemical species
a_1, b_1	Chemical species of A and B
B_0	Applied magnetic field
k_1, k_2	Rate constants
T_w	Temperature at the wall
T_∞, C_∞	Ambient temperature and concentration
a_0	Uniform concentration
T	Temperature
ρ_f	Density of the fluid
σ^*, k^*	Stefan–Boltzman constants
k	Thermal conductivity of the fluid
c_f	The specific heat of liquid
a, b, n	Physical quantities of Sisko fluid
D_A, D_B	Diffusion species coefficients of A and B
$(\rho c)_f$	Heat capacity of the base fluid
$(\rho c_p)_p$	Effective heat capacity of the fluid
f, g	Dimensionless stream functions
f', g'	Dimensionless velocities
θ, ϕ, h	Dimensionless temperature and concentrations
η	Dimensionless variable

1. Introduction

Fluid flow phenomenon presently plays a significant role in modern era of engineering and industrial applications. Meanwhile, flows of Newtonian and non-Newtonian fluids have acquired significant attention. Especially, the flow, heat and mass transfer due to stretched surfaces have gained much attraction in the progressive fields of chemical engineering and metallurgy process. Several researchers [1–8] studied Newtonian fluids to describe the features of flows. Moreover, the study of non-Newtonian fluid flows becomes essential in the modern world of science and technology. In this regard, Hayat *et al* [9] and Inan and Bahdir [10] studied the characteristics of non-Newtonian fluid flows. A lot of research related to the flow of non-Newtonian fluids concentrated on exploring the problem that explains both the properties of the fluid simultaneously, i.e., shear thinning and shear thickening characteristics of the fluid. In this regard, Sisko [11] proposed a model known as the Sisko fluid model which is generally used for the measurements on lubricating greases. This model is very significant because it can sketch many non-Newtonian fluid flows over the most important range of shear rates. Three-parameter Sisko fluid model can be considered as a generalisation of the Newtonian fluids and power-law fluids. Hayat *et al* [12] explored the flow of Sisko fluid in the porous medium. The boundary layer equation for Sisko fluid flow model was developed by Khan and Shahzad [13]. In this work, they addressed the analytical solution of the boundary layer equations and used the non-fractional values of the power-law index along with heat and mass transfer phenomena. Malik *et al* [14] investigated the convective flow due to a stretching surface with heat transfer in Sisko fluid. Munir *et al* [15] elucidated the 3D Sisko fluid flow and convective heat transfer mechanism over a stretched surface. The numerical illustration of Sisko fluid flow with Fourier's and Fick's laws is presented by Khan *et al* [16]. Moreover, the 3D Sisko nanofluid flow under convective conditions and magnetic field was considered by Hayat *et al* [17]. Recently, this model was used by Khan *et al* [18] to comput the numerical results with Cattaneo–Christov heat flux model and chemical reaction. Very recently, Khan *et al* [19] have considered this model to incorporate different effects which characterise the flow, heat and mass transfer mechanism with the help of different numerical approaches.

The process of synergies between two or more chemicals to produce one or more new chemical compound is known as chemical reaction. Based on the physical structure (i.e. length, weight, architectural pattern, colour, temperature, size, shape, distribution, language, disease, appearance, radioactivity, income etc.) the objects in such a reaction are described through heterogeneous and homogeneous reactions. Chemical reaction can appear on catalyst surface (heterogeneous situation of reactions) as well as in bulk (homogeneous situation of reactions). As the reactant product relies merely on the type of reactant species, homogeneous processes are simpler than heterogeneous processes. However, heterogeneous processes sustain practical significance as it communicates the dependency of the product on the type of distinct reactant species. Corrosion phenomenon, electrolytic cells and batteries involve such reactions. The models regarding heterogeneous and homogeneous situation of reactions with equal/unequal diffusivities are suggested by Chaudhary and Merkin [20,21]. Nandkeolyar *et al* [22] reported the importance of heterogeneous and homogeneous situations of reactions in stretchable flow of convective viscous liquid subject to viscous dissipation. Impact of non-Fourier theory in Williamson liquid flow through heterogeneous and homogeneous situations of reactions is addressed by Ramzan *et al* [23]. Qayyum *et al* [24] explored melting heat and inclined MHD aspects in chemically reacting hyperbolic-tangent liquid towards nonlinear moving surface.

Thermal radiation has a significant role in diverse high-temperature processes. It has numerous applications in different manufacturing industries for designing nuclear power plants. This concept is also prevalent in furnaces, boilers, engine cooling process and so on. Further, the thermal radiation effect has a pivotal role in space vehicles, nuclear plants, gas turbines, aircraft, devices for satellites etc. Rahman *et al* [25] examined the affect of heat transport on modified second grade liquid under thermal radiation. Kothandapani and Prakash [26] discussed the effects of thermal radiation on MHD flow of Williamson nanoliquid in an asymmetric channel. A good number of work on the influence of thermal radiation on flow and heat transfer can be found in [27–29] giving the impact of external agencies on the rate of flow and heat transfer.

The aforesaid studies regarding Sisko fluid model indicate that there is a huge gap which is not filled up until now. The purpose of the present investigation is to explore the 3D unsteady fluid flow over a bidirectional stretched surface in the presence of heterogeneous–homogeneous reaction, nonlinear thermal radiation and magnetic field. The nonlinear coupled ODEs are then considered for the numerical solution while using bvp4c in Matlab. The outcomes are displayed in the form of velocity, temperature and concentration profiles. Furthermore, all the physical quantities including skin friction and local Nusselt number are calculated in the tabular form. Present results are verified with the existing literature.

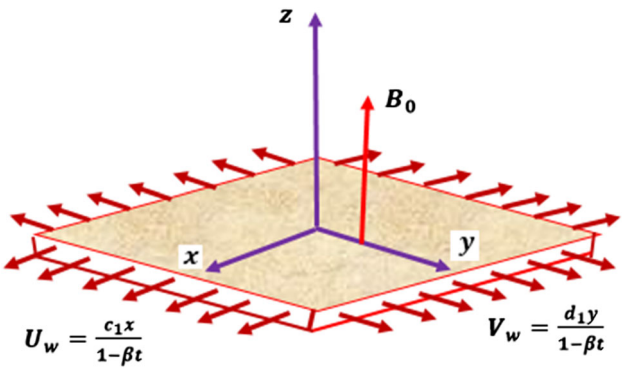

Figure 1. Physical diagram.

2. Problem description

Consider the unsteady 3D generalised Newtonian fluid flow with thermally radiative heat and chemically reacting mass transfer in the presence of magnetic field. The fluid flow due to the time-dependent stretching velocities at $z = 0$ are

$$u = \frac{c_1 x}{1-\beta t} \quad \text{and} \quad v = \frac{\mathrm{d}_1 y}{1-\beta t},$$

which are equal in magnitude but opposite in direction, i.e. u in the x-direction and v in y-direction. Uniform magnetic field is applied in the z-direction which is perpendicular to the x- and y-axes. The physical model is shown in figure 1. The stretching surface temperature is

$$T_w = T_\infty + \frac{\mathrm{d}x}{1-\beta t}$$

and the concentration of the fluid at the stretching surface is kept constant. The ambient temperature and concentration of the fluid away from the surface are taken as T_∞ and C_∞, respectively.

To incorporate the chemical reaction, namely heterogeneous–homogeneous, in the flow problem, Chaudhary and Merkin [20,21] introduced a simple interaction between homogeneous (bulk) and heterogeneous (surface reaction) reactions evolving the two chemical species A and B. This interaction is further defined as follows:

$$A + 2B \to 3B, \quad \text{rate} = k_1 a_1 b^2, \tag{1}$$

$$A \to B, \quad \text{rate} = k_2 a_1. \tag{2}$$

The chemical reaction will possess constant temperature due to thermal equilibrium property of the heat flux (heat transfer out and heat transfer in). In the absence of autocatalyst B, the uniform concentration a_0 of A will take place instead of a_1.

By using the boundary layer approximations and the aforementioned assumption, the continuity, momentum, temperature and concentration equations are reduced in the following form:

$$\frac{\partial u}{\partial x} + \frac{\partial v}{\partial y} + \frac{\partial w}{\partial z} = 0, \tag{3}$$

$$\frac{\partial u}{\partial t} + u\frac{\partial u}{\partial x} + v\frac{\partial u}{\partial y} + w\frac{\partial u}{\partial z} = \frac{a}{\rho_f}\frac{\partial^2 u}{\partial z^2} - \frac{b}{\rho_f}\frac{\partial}{\partial z}\left(-\frac{\partial u}{\partial z}\right)^n - \frac{\sigma B_0^2}{\rho_f}u, \tag{4}$$

$$\frac{\partial v}{\partial t} + u\frac{\partial v}{\partial x} + v\frac{\partial v}{\partial y} + w\frac{\partial v}{\partial z} = \frac{a}{\rho_f}\frac{\partial^2 v}{\partial z^2} + \frac{b}{\rho_f}\frac{\partial}{\partial z}\left(-\frac{\partial u}{\partial z}\right)^{n-1}\frac{\partial v}{\partial z} - \frac{\sigma B_0^2}{\rho_f}v, \tag{5}$$

$$\frac{\partial T}{\partial t} + u\frac{\partial T}{\partial x} + v\frac{\partial T}{\partial y} + w\frac{\partial T}{\partial z} = \alpha_1\frac{\partial^2 T}{\partial z^2} - \frac{1}{(\rho c)_f}\frac{\partial q_r}{\partial z}, \tag{6}$$

$$\frac{\partial a_1}{\partial t} + u\frac{\partial a_1}{\partial x} + v\frac{\partial a_1}{\partial y} + w\frac{\partial a_1}{\partial z} = D_A\left(\frac{\partial^2 a_1}{\partial z^2}\right) - k_1^* a_1 b_1^2, \tag{7}$$

$$\frac{\partial b_1}{\partial t} + u\frac{\partial b_1}{\partial x} + v\frac{\partial b_1}{\partial y} + w\frac{\partial b_1}{\partial z} = D_B\left(\frac{\partial^2 b_1}{\partial z^2}\right) + k_1^* a_1 b_1^2. \tag{8}$$

Equations (4)–(8) are subjected to the following boundary conditions:

$$\begin{aligned} &u = U_w = \frac{c_1 x}{1-\beta t}, \quad v = V_w = \frac{\mathrm{d}_1 y}{1-\beta t}, \\ &w = 0, \quad T = T_w, \\ &D_A\left(\frac{\partial a_1}{\partial z}\right) = k_1 a_1, \\ &D_B\left(\frac{\partial b_1}{\partial z}\right) = -k_2 a_1 \qquad \text{at } z = 0, \end{aligned} \tag{9}$$

$$u \to 0, \quad v \to 0, \quad T \to T_\infty, \quad a_1 \to a_0, \quad b_1 \to 0 \qquad \text{as } z \to \infty. \tag{10}$$

The governing eqs (4)–(8) subjected to the boundary conditions (9) and (10) can be expressed in a simpler form by introducing the following transformations:

$$u = \frac{c_1 x}{1-\beta t} f'(\eta), \quad v = \frac{c_1 y}{1-\beta t} g'(\eta),$$

$$w = -c_1\left(\frac{c^{n-2}}{\rho_f/b}\right)^{1/(n+1)}\left[\frac{2n}{n+1}f(\eta) + \frac{1-n}{1+n}\eta f'(\eta) + g(\eta)\right]$$

$$\times x^{(n-1)/(n+1)}\,(1-\beta t)^{(1-2n)/(n+1)},$$

$$\theta(\eta)=\frac{T-T_\infty}{T_w-T_\infty},\quad \eta=z\left(\frac{c^{2-n}}{b/\rho_f}\right)^{1/(n+1)}\times x^{(1-n)/(1+n)}\,(1-\beta t)^{(n-2)/(n+1)}. \tag{11}$$

In view of eq. (11), we obtain the following set of nonlinear ordinary differential equations with respect to the dimensionless variable η:

$$Af'''-S\left[f'+\frac{2-n}{1+n}\eta f''\right]+n(-f'')^{n-1}f''' +\left(\frac{2n}{n+1}\right)ff''-f'^2+gf''-M^2f'=0, \tag{12}$$

$$Ag'''-S\left[g'+\frac{2-n}{1+n}\eta g''\right] +(-f'')^{n-1}g'''-(n-1)g''f'''(-f'')^{n-2} +\left(\frac{2n}{n+1}\right)fg''-g'^2+gg''-M^2g'=0, \tag{13}$$

$$\left[\left\{1+R_d(1+(\theta_w-1)\theta)^3\right\}\theta'\right]' +\Pr\left(\frac{2n}{n+1}f+g\right)\theta'-\Pr S\left[\theta+\frac{2-n}{1+n}\eta\theta'\right] -\Pr f'\theta=0, \tag{14}$$

$$\phi''+\mathrm{Sc}\left(\frac{2n}{n+1}f+g\right)\phi'-\mathrm{Sc}S\left(\frac{2-n}{1+n}\eta\phi'\right) -\mathrm{Sc}k_1(1-\phi)^2\phi=0. \tag{15}$$

The dimensionless boundary conditions are

$$f(0)=0,\quad g(0)=0,\quad f'(0)=1,$$

$$g'(0)=\lambda,\quad \theta(0)=1,\quad \phi'(0)=k_2\phi(0), \tag{16}$$

$$f'\to 0,\quad g'\to 0,\quad \theta\to 0,\quad \phi\to 1 \text{ as } \eta\to\infty. \tag{17}$$

In the above equations, prime denotes the differentiation with respect to η.

The Rosseland approximation used in eq. (6) leads to the following expression:

$$q_r=-\frac{4\sigma^*}{3k^*}\frac{\partial T^4}{\partial z}=-\frac{16\sigma^*}{3k^*}T^3\frac{\partial T}{\partial z}. \tag{18}$$

The linearised Rosseland approximation is a simple approach towards the thermal radiation problem, where additional computations or analytical struggles are not required. For nonlinear thermal radiation, some analytical efforts must be performed for simplification of the aforementioned relation. An additional temperature ratio parameter θ_w will occur and due to this reason the energy equation will be more nonlinear. Thus, by using eq. (18) in eq. (6), we obtained eq. (14).

Diffusion coefficients of chemical species A and B are assumed to be of comparable size. Then the following relation will be obtained:

$$\phi(\eta)+h(\eta)=1. \tag{19}$$

The above relation is further a neccessary condition to get eq. (15).

The dimensionless flow parameters are illustrated as below:

$A=\frac{\mathrm{Re}_b^{\frac{2}{n+1}}}{\mathrm{Re}_a}$	Material parameter of the Sisko fluid
$\mathrm{Re}_a=\frac{U_w x\rho_f}{a}$, $\mathrm{Re}_b=\frac{U_w^{2-n}x^n\rho_f}{b}$	Local Reynold numbers
$M^2=\frac{\sigma B_0^2}{(\rho c)_f}$	Magnetic parameter
$\Pr=\frac{xU_w}{\alpha_1}\mathrm{Re}_b^{-\frac{2}{n+1}}$	Generalised Prandtl number
$\lambda=\frac{d_1}{c_1}$	Ratio parameter of stretching rates
$\mathrm{Sc}=\frac{xU_w}{D_A}\mathrm{Re}_b^{-\frac{2}{n+1}}$	Schmidt number
$k_1=\frac{a_0^2k_1^*x}{U_w}$	Strength of homogeneous reaction
$k_2=\frac{k_2^*c_1x}{D_A}\mathrm{Re}_b^{-\frac{1}{n+1}}$	Strength of heterogeneous reaction
$S=\frac{\beta}{c_1}$	Unsteadiness parameter
$R_d=\frac{16\sigma^*T_\infty^3}{3k^*k}$	Radiation parameter
$\theta_w=\frac{T_w}{T_\infty}$	Temperature ratio parameter

3. Physical quantities

Physical quantities appeared in the chemically reactive and nonlinear thermally radiative 3D unsteady flow of magneto-Sisko fluid in the presence of magnetic field accounting all physical quantities are as follows. Main focus under consideration are the resistive forces, namely skin friction and rate of mass transfer (local Nusselt number). These physical quantities are computed in the tabular form for both shear thinning fluid and shear thickening fluid.

The aforesaid dimensionless relations are defined as

$$\frac{1}{2}\mathrm{Re}_b^{1/(n+1)}C_{fx}=Af''(0)-(-f''(0))^n, \tag{20}$$

$$\frac{1}{2}\mathrm{Re}_b^{1/(n+1)}C_{fy}=\frac{V_w}{U_w}\left[Ag''(0)+(-f''(0))^{(n-1)}g''(0)\right], \tag{21}$$

$$\mathrm{Re}^{-1/(n+1)}\mathrm{Nu}_x=-\left[1+R_d\{1+(\theta_w-1)\theta(0)\}^3\right]\theta'(0). \tag{22}$$

4. Numerical scheme

Thermally radiative 3D unsteady magneto-Sisko fluid flow with heterogeneous–homogeneous reaction is presented in eqs (12)–(15) with associated boundary conditions (16) and (17) for numerical computation. The numerical technique implemented in this study is usually known as finite difference Lobatto IIIA formula for accuracy up to fourth order. The tolerance related to this accuracy has been determined as 10^{-6}. The main steps for this scheme is as follows:

$$f = F_1, \quad f' = F_2, \quad f'' = F_3, \quad f''' = F_3', \tag{23}$$
$$g = F_4, \quad g' = F_5, \quad g'' = F_6, \quad g''' = F_6', \tag{24}$$
$$\theta = F_7, \quad \theta' = F_8, \quad \theta'' = F_8', \tag{25}$$
$$\phi = F_9, \quad \phi' = F_{10}, \quad \phi'' = F_{10}', \tag{26}$$

where

$$F_3' = \frac{S\left[F_2 + \left(\frac{2-n}{1+n}\right)\eta F_3\right] - \left(\frac{2n}{1+n}\right)F_1F_3 + F_2^2 - F_4F_3 + M_2^2F_2}{A + n\,(-F_3)^{n-1}}, \tag{27}$$

$$F_6' = \frac{S\left[F_5 + \left(\frac{2-n}{1+n}\right)\eta F_6\right] + \left[(n-1)\,F_3'\,(-F_3)^{n-2} - \left(\frac{2n}{1+n}\right)F_1 - F_4\right]F_6 + F_5^2 + F_5^2F}{A + (-F_3)^{n-1}}, \tag{28}$$

$$F_8' = \frac{-\Pr\left[\left(\frac{2n}{1+n}\right)F_1 + F_4\right]F_8 + \Pr S\left(F_7 + \frac{2-n}{1+n}\eta F_8\right) - \Pr F_2F_7}{(1 + R_d(1 + (\theta_w - 1)F_7)^3)}, \tag{29}$$

$$F_{10}' = -\mathrm{Sc}\left[\left(\frac{2n}{1+n}\right)F_1 + F_4\right]F_{10} + \mathrm{Sc}\,S\left(\frac{2-n}{1+n}\right)\eta F_{10} - \mathrm{Sc}\,k_1(1-F_9)^2F_9, \tag{30}$$

with the associated boundary conditions

$$F_0(1) = 0, \quad F_0(2) = 1, \quad F_\infty(2) = 0, \tag{31}$$
$$F_0(4) = 0, \quad F_0(5) = \lambda, \quad F_\infty(5) = 0, \tag{32}$$
$$F_0(8) = 1, \quad F_0(10) = k_2F_0(9), \tag{33}$$
$$F_\infty(7) = 0, \quad F_\infty(9) = 1. \tag{34}$$

5. Validation of scheme

The computations presented in this study are validated using tabular values of the local skin friction and local Nusselt number as shown in tables 1 and 2. This comparison incorporates the effect of λ on the local skin friction, keeping the other parameters fixed. These tabular values show an excellent agreement between bvp4c routine and shooting technique with RK-45 Fehlberg method. Another comparison of the present analysis with the previously published work by Malik *et al* [14] shows a very good correlation with each other and is presented in table 3.

6. Computational results and discussion

A numerical technique is followed to examine the impact of different governing parameters in the flow eqs (12) to (15) with associated boundary conditions (16) and (17). The present investigation is about the effect of heterogeneous–homogeneous reaction together with nonlinear thermal radiation on the 3D unsteady magneto-Sisko fluid flow. Various dimensionless quantities are tested for their effects on the graphs of velocity, temperature and concentration distributions and the numerical values of local skin friction and local Nusselt number tabulated. These governing parameter are: the material parameter (A), unsteadiness parameter (S), magnetic parameter (M), power law-index (n), Prandtl number (Pr), stretching ratio parameter (λ), thermal radiation parameter (R_d), temperature ratio parameter (θ_w), Schmidt number (Sc), homogeneous parameter (k_1) and heterogeneous parameter (k_2).

6.1 *Local skin friction and Nusselt number*

6.1.1 *Impact of M and S on local skin friction.* The local skin frictions are presented in tables 4 and 5. The local skin friction in both cases of power-law fluids with the properties of pseudoplastic fluid and dilatant fluid is found to be an increasing order with the increasing values of M and S. The physical perspective in this regards indicates that the flow resistance is due to Lorentz forces generated by magnetic field.

6.1.2 *Impact of R_d and θ_w on local Nusselt number.* The influence of R_d and θ_w on the local Nusselt number in the case of pseudoplastic fluid and dilatant fluid is presented in table 6. The rate of heat transfer in favour of these parameters is enhanced. Physical significance concerning this effect shows that when radiation is applied,

Table 1. Comparison of bvp4c and shooting technique, when $A = 0.2, S = 0.2, M = 0.2, R_d = 1.0, \Pr = 1.2, \theta_w = 1.2, k_1 = 0.2, k_2 = 0.6$ and $\mathrm{Sc} = 1.0$.

$-\frac{1}{2}\mathrm{Re}_b^{1/(n+1)} C_{fx}$				
Parameter	bvp4c		Shooting method	
λ	$n = 0.8$	$n = 1.8$	$n = 0.8$	$n = 1.8$
0.2	1.245485	1.210381	1.245485	1.21038
0.4	1.27748	1.254568	1.27748	1.254567
0.6	1.308056	1.29697	1.308056	1.29697
$-\frac{1}{2}\mathrm{Re}_b^{1/(n+1)} C_{fy} \left(\frac{U_w}{V_w}\right)$				
Parameter	bvp4c		Shooting method	
λ	$n = 0.8$	$n = 1.8$	$n = 0.8$	$n = 1.8$
0.2	0.1874347	0.1885341	0.1874348	0.1885339
0.4	0.4257742	0.4257988	0.4257743	0.4257985
0.6	0.7052276	0.7056185	0.7052277	0.7056181

Table 2. Comparison of bvp4c and shooting technique, when $A = 0.2, S = 0.2, M = 0.2, \lambda = 0.5, \Pr = 1.2, \theta_w = 1.2, k_1 = 0.2, k_2 = 0.6$ and $\mathrm{Sc} = 1.0$.

$-\mathrm{Re}_b^{1/(n+1)} \mathrm{Nu}_x$				
Parameter	bvp4c		Shooting method	
R_d	$n = 0.8$	$n = 1.8$	$n = 0.8$	$n = 1.8$
1.0	1.815448	1.919434	1.815448	1.919434
1.2	1.891554	1.992434	1.891554	1.992434
1.4	1.961893	2.059251	1.961893	2.059251

Table 3. Comparison of the present work with the previous results, when $S = \lambda = 0.0$.

$-\frac{1}{2}\mathrm{Re}_b^{1/(n+1)} C_f$		
n	Present results	Malik *et al* [14]
1.0	2.000008	2.00000
2.0	1.914495	1.914495
3.0	1.875080	1.875081

Table 4. The variation of local skin friction coefficient with A, S, M and λ, when $\Pr = 1.2$, $R_d = 1.0, \theta_w = 1.2, k_1 = 0.2, k_2 = 0.6$ and $\mathrm{Sc} = 1.0$.

				$-\frac{1}{2}\mathrm{Re}_b^{1/(n+1)} C_{fx}$	
A	S	M	λ	$n = 0.8$	$n = 1.8$
0.1	0.2	0.2	0.5	1.235467	1.229421
0.3				1.34679	1.321894
0.5				1.448259	1.411706
0.1	0.0	0.2	0.5	1.180555	1.142934
	0.1			1.20795	1.186503
	0.2			1.235467	1.229421
0.1	0.2	0.0	0.5	1.217823	1.211355
		0.2		1.235467	1.229421
		0.4		1.286565	1.282907
0.1	0.2	0.2	0.2	1.190714	1.164741
			0.4	1.220898	1.208323
			0.6	1.249739	1.250132

the temperature of the fluid increases. Impact of temperature ratio parameter on the rate of heat transfer is due to the higher fluid temperature compared to ambient temperature.

6.2 *Velocity profile*

6.2.1 *Influence of M on $f'(\eta)$ and $g'(\eta)$.* Influence of increased values of M on velocity components $f'(\eta)$ and $g'(\eta)$ for both pseudoplastic fluid and dilatant fluid is observed in the diminishing behaviour shown in figures 2a and 2b. Associated boundary layer thickness also reduces. Physically, Lorentz forces are increasing when the magnetic field increases and as a result the velocity of the fluid reduces.

6.3 *Temperature profile*

6.3.1 *Influence of A and θ_w on $\theta(\eta)$.* In figure 3a, a decrease in temperature profiles is seen for increasing values of A for pseudoplastic fluid as well as dilatant fluid. The thermal boundary layer is also found to reduce. Results obtained while portraying this figure is more noticeable in the pseudoplastic fluid condition.

Table 5. The variation of local skin friction coefficient with A, S, M and λ, when Pr $= 1.2$, $R_d = 1.0$, $\theta_w = 1.2$, $k_1 = 0.2$, $k_2 = 0.6$ and Sc $= 1.0$.

				$-\frac{1}{2}\mathrm{Re}_b^{1/(n+1)} C_{fy}(U_w/V_w)$	
A	S	M	λ	$n = 0.8$	$n = 1.8$
0.1	0.2	0.2	0.5	0.5362644	0.5399272
0.3				0.5841034	0.5811563
0.5				0.6277770	0.6211994
0.1	0.0	0.2	0.5	0.5257358	0.4933554
	0.1			0.5283926	0.5168608
	0.2			0.5362644	0.5399272
0.1	0.2	0.0	0.5	0.5257358	0.5302135
		0.2		0.5362644	0.5399272
		0.4		0.5663981	0.5603459
0.1	0.2	0.2	0.2	0.1794329	0.1812007
			0.4	0.4072864	0.4098021
			0.6	0.6741979	0.6798624

Table 6. The variation of local Nusselt number with A, S, M, λ, Pr, R_d and θ_w, when $k_1 = 0.2$, $k_2 = 0.6$ and Sc $= 1.0$.

							$-\mathrm{Re}_b^{-1/(n+1)} Nu_x$	
A	S	M	λ	Pr	R_d	θ_w	$n = 0.8$	$n = 1.8$
0.1	0.2	0.2	0.5	1.2	1.0	1.2	1.791724	1.823125
0.3							1.835962	1.868718
0.5							1.871799	1.906778
0.1	0.0	0.2	0.5	1.2	1.0	1.2	1.690877	1.638012
	0.1						1.740617	1.735306
	0.2						1.791724	1.823125
0.1	0.2	0.0	0.5	1.2	1.0	1.2	1.80152	1.827276
		0.2					1.791724	1.823125
		0.4					1.763769	1.811025
0.1	0.2	0.2	0.2	1.2	1.0	1.2	1.720181	1.751024
			0.4				1.768489	1.799538
			0.6				1.814445	1.846328
0.1	0.2	0.2	0.5	0.8	1.0	1.2	1.376801	1.38432
				1.0			1.592817	1.612378
				1.2			1.791724	1.823125
0.1	0.2	0.2	0.5	1.2	1.0	1.2	1.791724	1.823125
					1.2		1.865334	1.886941
					1.4		1.933073	1.945582
0.1	0.2	0.2	0.5	1.2	1.0	1.2	1.791724	1.892808
						1.4	1.943122	2.038512
						1.6	2.102364	2.187498

From the physical point of view, the diminishing effect in the consistency index, i.e. viscosity of the fluid is due to the higher values of A. Figure 3b shows the effect of increasing values of θ_w on $\theta(\eta)$. The associated thermal boundary layer thickness is found to be in the escalating order. Both cases of this fluid model, i.e., shear thickening and shear thickening, are tested,

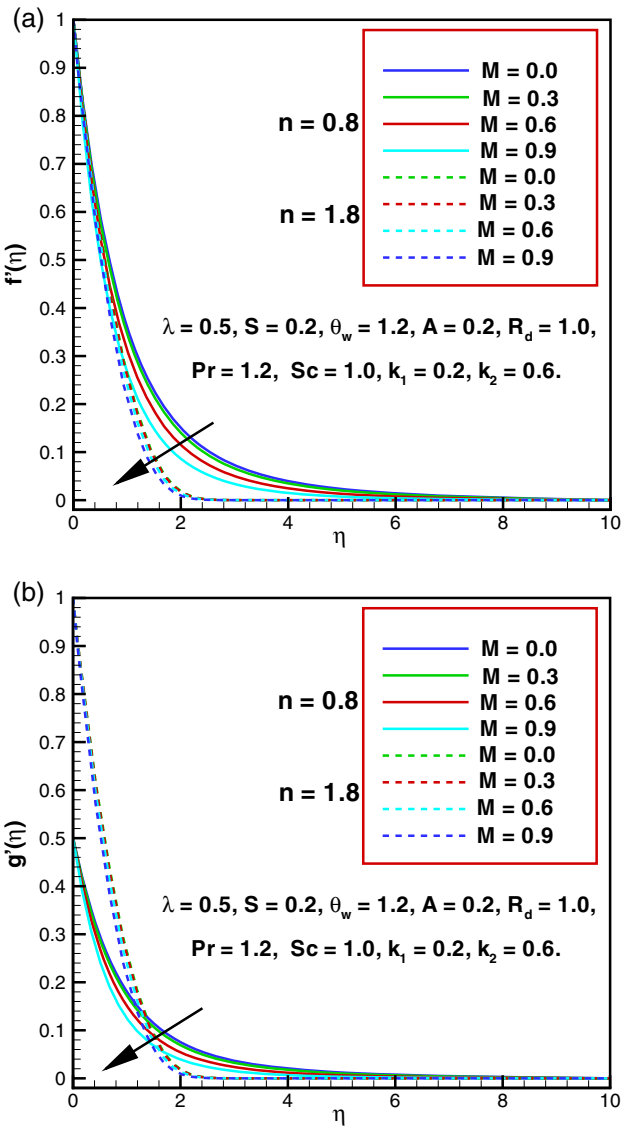

Figure 2. Influence of magnetic parameter M on velocity components (**a**) $f'(\eta)$ and (**b**) $g'(\eta)$.

but a remarkable result is noticed in the shear thinning case. The enhancement in temperature of such a fluid model is due to the temperature ratio parameter and because of the large value of the fluid temperature.

6.3.2 *Influence of* Pr *and* R_d *on* $\theta(\eta)$. By utilising both shear thinning and shear thickening, $\theta(\eta)$ and the associated thermal boundary layer thickness are continuously decreasing within the boundary layer with the increasing values of Pr and is demonstrated in figure 4a. This shows that the rate of cooling is faster in the case of higher Prandtl number and so the temperature is decreasing at a faster rate. The significant effect of the higher values of R_d on $\theta(\eta)$ is sketched in figure 4b. Physically, this

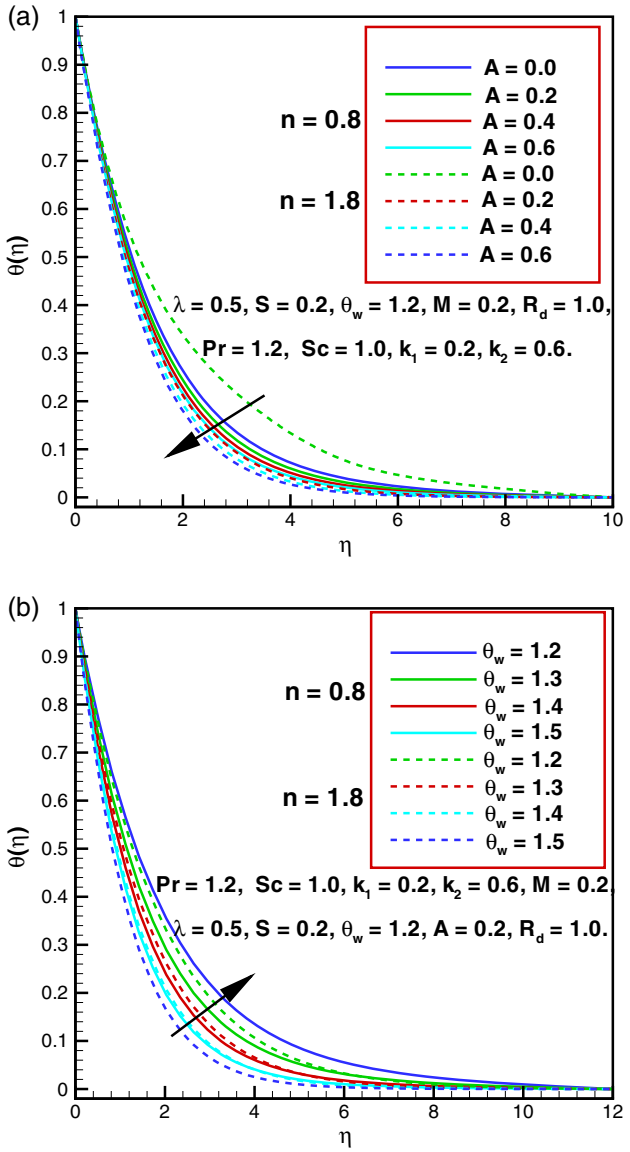

Figure 3. Influence of (**a**) material parameter A and (**b**) temperature ratio parameter θ_w on temperature.

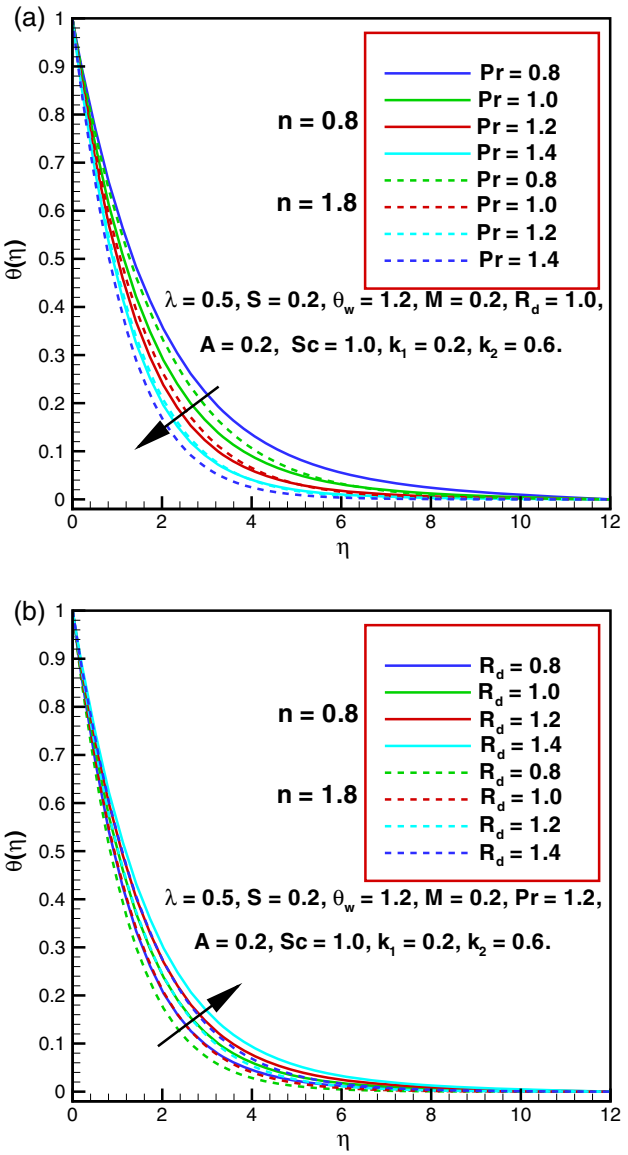

Figure 4. Influence of (**a**) Prandtl number Pr and (**b**) thermal radiation parameter R_d on temperature.

effect indicates that radiation supplied to the fluid flow will enhance the rate of heat transfer and as a result the temperature of the fluid increases.

6.3.3 *Influence of M and λ on $\theta(\eta)$.* Figure 5a elucidates the impact of M on $\theta(\eta)$ for both pseudoplastic and dilatant fluids and a remarkable increase in the temperature of fluid. The relevant thermal boundary layer thickness also increases for higher values of M. This increase in fluid temperature is accountable for the enrichment of Lorentz forces. Another important behaviour of the increasing values of λ on $\theta(\eta)$ is portrayed in figure 5b, where the temperature of the fluid decreases. This effect is due to the increase in distance between the fluid particles and as a result the heat transfer rate will slow down.

6.4 *Concentration profile*

6.4.1 *Influence of λ and* Sc *on $\phi(\eta)$.* In figures 6a and 6b, the concentration $\phi(\eta)$ of the fluid flow is observed in enhancing conduct while testing both the conditions, i.e. pseudoplastic fluid and dilatant fluid with variation of λ and Sc. This effect is observed within the boundary layer and the associated boundary layer thickness is also increased. Figure 6a displays the increase in the concentration of the fluid due to the higher values of stretching ratio parameter. More stretching of the surface will increase the mass transfer rate. Figure 6b shows

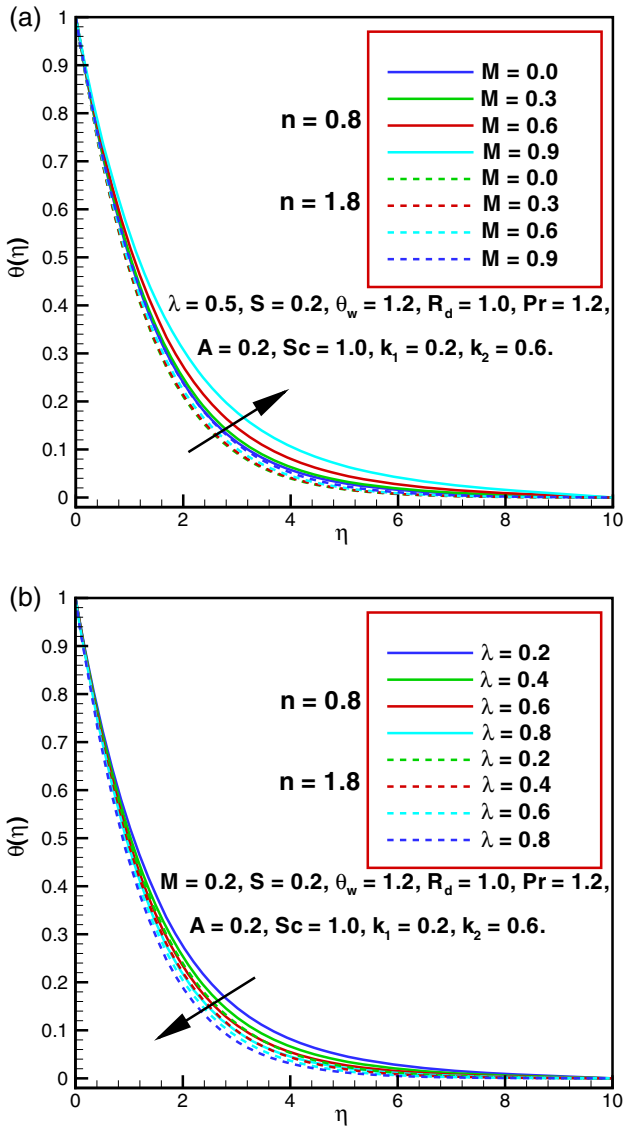

Figure 5. Influence of (**a**) magnetic parameter M and (**b**) stretching ratio parameter λ on temperature.

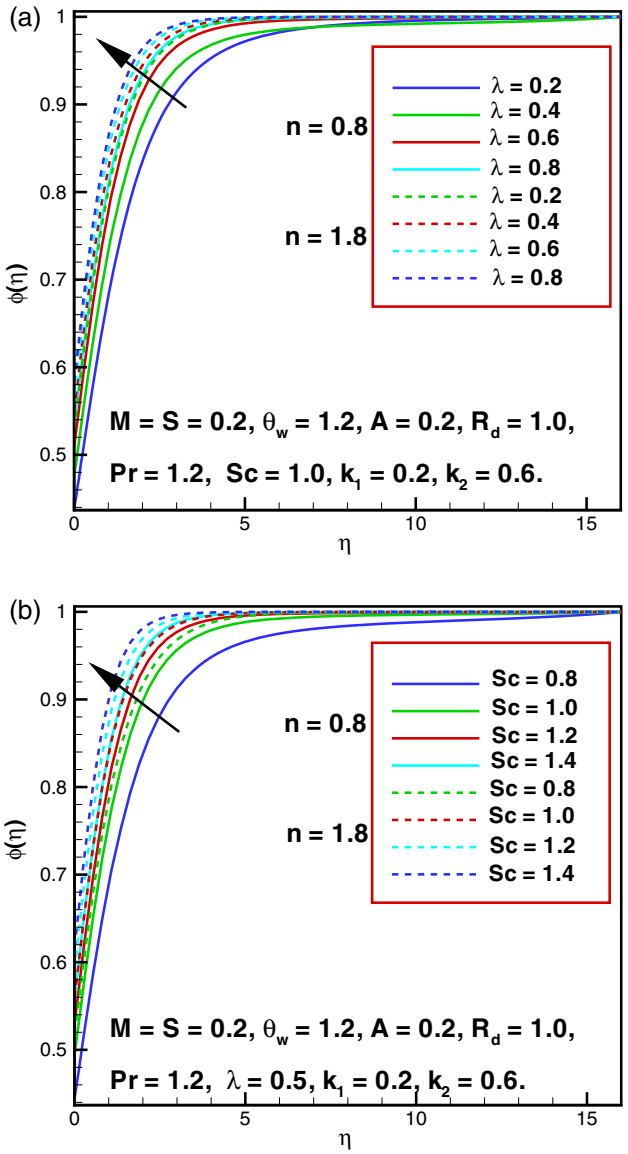

Figure 6. Influence of (**a**) stretching ratio parameter λ and (**b**) Schmidt number Sc on concentration.

the impact of Sc on $\phi(\eta)$ and this effect is because of the ratio of viscous diffusion rate and molecular diffusion rate. Thus, increase in the value of Sc will enhance the concentration profile.

6.4.2 *Influence of S and M on $\phi(\eta)$.* Impact of S on $\phi(\eta)$ is demonstrated in figure 7a and an enhancement in $\phi(\eta)$ is found for increasing values of S. This effect is utilised in both cases, i.e., pseudoplastic and dilatant fluids. In both cases, the concentration and boundary layer thickness increase. Effect of M on $\phi(\eta)$ is illustrated in figure 7b. The concentration profile and the associated boundary layer diminish for increasing values of M. The Lorentz forces introduced with the help of M while plotting the concentration distribution causes a resistive drag force and as a result less mass will be transferred.

6.4.3 *Influence of k_1 and k_2 on $\phi(\eta)$.* The impacts of k_1 and k_2 on $\phi(\eta)$ are shown in figures 8a and 8b. From these figures, a decline is observed. The graphs displayed are further tested for both cases, i.e., shear thinning and shear thickening. Whereas the associated boundary layer thickness of reactants is reported in the increasing custom. Because the concentration of the fluid is blown away from the surface. Reduction in $\phi(\eta)$ for both reactant parameters k_1 and k_2 is because of the dominance of diffusion coefficients reaction rates. From the physical point of view, such types of rates of mass transfer shows a significant impact.

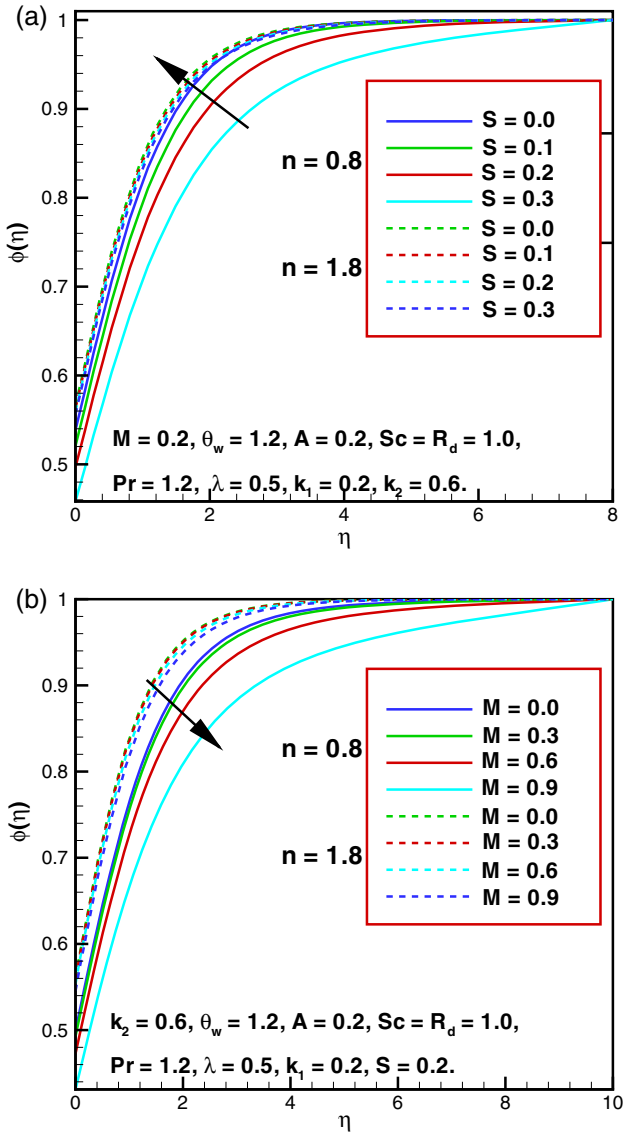

Figure 7. Influence of (**a**) unsteadiness parameter S and (**b**) magnetic parameter M on concentration.

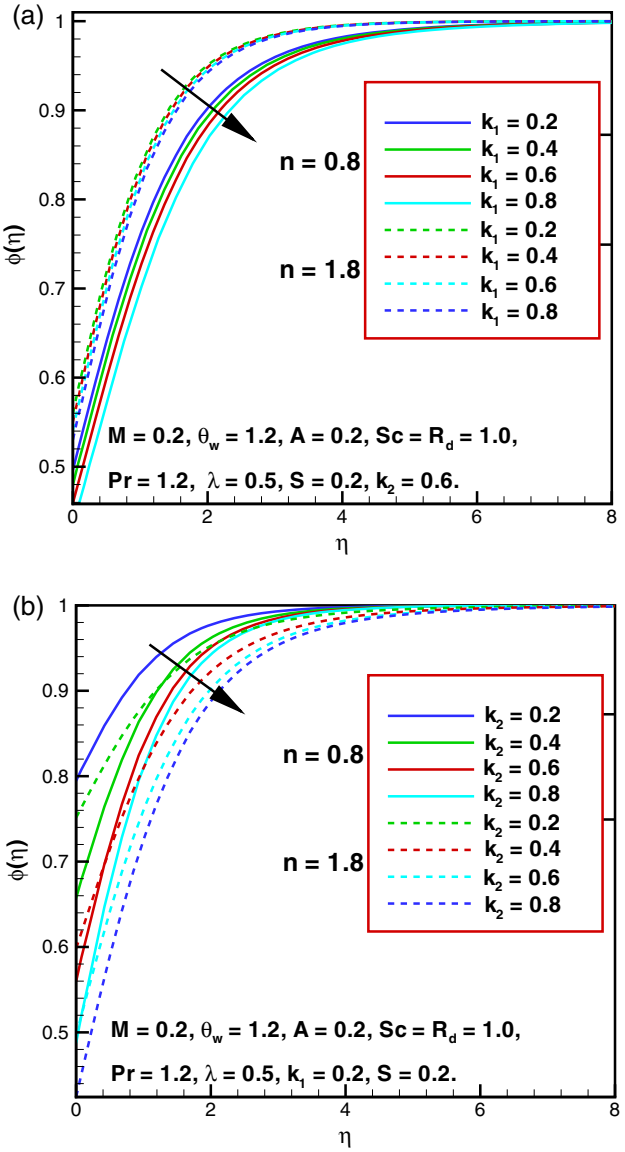

Figure 8. Influence of (**a**) homogeneous strength parameter k_1 and (**b**) heterogeneous parameter k_2 on concentration.

7. Conclusions

In this article, the numerical simulation of the nonlinear thermal radiative 3D unsteady Sisko fluid flow in the presence of heterogeneous–homogeneous reaction and magnetic field is demonstrated. The flow of the fluid is generated with the help of bidirectional stretching surface. The energy and concentration equations were utilised to explore the heat and mass transfer phenomena in detail up to some extent. All the results of this illustration are presented in tabular and graphical forms. Results of the present work are validated using another numerical technique called shooting method. Furthermore, a comparison was done to verify the present results with the published work and both results are found to agree with each other. However, some major surprising results are highlighted in the following paragraph.

Our analysis showed that the nonlinear thermal radiative parameter R_d enhanced the temperature of the fluid. Similarly, the temperature ratio parameter θ_w caused the boosting in temperature profile. These effects were true for both shear thinning and shear thickening fluids. It was also noted that the concentration at the surface decreased with the strength of the reactant parameters of homogeneous and heterogeneous reactions. The solute concentration was, however, increased with the stretching parameter. Additionally, the concentration on the wall was incremented in the flow with the increase in the unsteadiness parameter.

References

[1] O Prakash and D Kumar, *Pramana – J. Phys.* **6**(**79**), 1457 (2012)
[2] N Sandeep and V Sugunamma, *World Appl. Sci. J.* **22**(**7**), 975 (2013)
[3] T Hayat, M Iqbal, H Yasmin, F E Alsaadi and H Gao, *Pramana – J. Phys.* **85**(**1**), 125 (2015)
[4] N Sandeep and C Sulochana, *Alex. Eng. J.* **55**(**2**), 819 (2016)
[5] N C Peddisetty, *Pramana – J. Phys.* **87**(**2**), 20 (2016)
[6] N Sandeep and M S Jagadeesh , *J. Appl. Fluid Mech.* **9**(**5**), 2205 (2016)
[7] N Sandeep, *Adv. Powder Technol.* **28**(**3**), 865 (2017)
[8] M Jayachandra Babu and N Sandeep, *Alex. Eng. J.* **55**(**3**), 2193 (2016)
[9] T Hayat, M Waqas, A Shehzad and A Alsaedi, *Pramana – J. Phys.* **86**(**1**), 3 (2016)
[10] B Inan and A R Bahdir, *Pramana – J. Phys.* **81**(**4**), 547 (2013)
[11] A W Sisko, *Ind. Eng. Chem. Res*. **50**, 1789 (1958)
[12] T Hayat, R J Moitsheki and S Abelman, *Appl. Math. Comput.* **217**(**2**), 622 (2010)
[13] M Khan and A Shahzad, *Quaest. Math.* **3**, 137 (2013)
[14] R Malik, M Khan, A Munir and W A Khan, *PLoS One* **9**(**10**), e107989 (2014)
[15] A Munir, A Shahzad and M Khan, *PLoS One* **10**, e0130342 (2015)
[16] W A Khan, M Khan, A S Alshomrani and L Ahmad, *J. Mol. Liq.* **224**, 1016 (2016)
[17] T Hayat, T Muhammad, S A Shehzad and A Alsaedi, *Adv. Powder Technol.* **27**, 504 (2016)
[18] M Khan, L Ahmad, A A Alshomrani, A K Alzahrani and M S Alghamdi, *J. Mol. Liq.* **238**, 19 (2017)
[19] M Khan, L Ahmad and W A Khan, *J. Braz. Soc. Mech. Sci. Eng.* **39**, 4475 (2017)
[20] M A Chaudhary and J H Merkin, *Fluid Dyn. Res.* **16**, 311 (1995)
[21] M A Chaudhary and J H Merkin, *Fluid Dyn. Res.* **16**, 335 (1995)
[22] R Nandkeolyar, S S Mosta and P Sibanda, *J. Nanotechnol. Eng. Med*. **4**, 041001 (2014)
[23] M Ramzan, M Bilal and J D Chung, *J. Mol. Liq.* **225**, 856 (2017)
[24] S Qayyum, R Khan and H Habib, *Int. J. Mech. Sci.* **133**, 1 (2017)
[25] M Rahman, M Manzur and M Khan, *J. Mol. Liq.* **223**, 217 (2016)
[26] M Kothandapani and J Prakash, *Int. J. Heat Mass Transfer* **81**, 234 (2015)
[27] M A Seddeek and A M Abdel, *Phys. Lett. A* **348**, 172 (2006)
[28] M Khan, M Irfan and W A Khan, *Int. J. Mech. Sci*. **130**, 375 (2017)
[29] M Khan, M Irfan, W A Khan and L Ahmad, *Res. Phys.* **7**, 1899 (2017)